Viking S-Band Doppler RMS Phase Fluctuations Used to Calibrate the Mean 1976 Equatorial Corona

A. L. Berman
TDA Engineering Office

J. A. Wackley
DSN Network Operations Section

Viking S-band doppler rms phase fluctuations (noise) and comparisons of Viking doppler noise to Viking differenced S-X range measurements are used to construct a mean equatorial electron density model for 1976:

$$N_e(r) = \frac{2.39 \times 10^8}{r^6} + \frac{1.67 \times 10^6}{r^{2.30}}$$

where N_e is in electrons/cm^3 and r is heliocentric distance in solar radii. The model yields at 1 AU:

$$N_e(214) = 7.3 \text{ electrons/cm}^3$$

Using Pioneer doppler noise results (at high heliographic latitudes, also from 1976), an equivalent nonequatorial electron density model is approximated as:

$$N_e(r,\phi_s) = \left\{ \frac{2.39 \times 10^8}{r^6} + \frac{1.67 \times 10^6}{r^{2.30}} \right\} 10^{-0.9(|\phi_s|/90)}$$

where ϕ_s is the heliographic latitude in degrees.

I. Introduction

Since early 1975, doppler noise (rms phase fluctuations) from the Pioneer and Helios spacecraft has been shown (Refs. 1 through 9) to be well represented functionally by integrated signal path electron density. Recently, a large data base of Viking doppler noise data has been accumulated and, as expected, is also well represented functionally by integrated signal path electron density. In companion articles in this volume, the radial dependence of electron density in the extended corona is refined (Ref. 1), and the actual numerical relationship between doppler noise and integrated signal path electron density is calculated via comparison of doppler noise to concurrent measurements of differenced S-X range (Ref. 2). In this article, a combined data set of all pass-average doppler noise values (from Helios 1, Helios 2, and Viking) computed

for impact parameters of between 2 and 4 solar radii is used to refine the coefficient of the inner corona electron density term ($\sim 1/r^6$). Combining this result with those of the companion articles, a newly calibrated mean equatorial electron density model is constructed for the last half of 1976. In addition, the topics of correlation of electron density with Earth-observed solar activity and functional dependence of electron density with heliographic latitude are briefly examined.

II. The Data Base

871 points of "pass-average" Viking two-way S-band doppler noise were accumulated during the following time period:

$$168 \leqslant \text{Day of Year (DOY), } 1976 \leqslant 355$$

and for the following range of Sun-Earth-Probe (SEP) angles:

$$00.58 \leqslant \text{SEP, degrees} \leqslant 54.13$$

The data were collected from all DSSs and for all (4) Viking spacecraft. "Pass-average" doppler noise is abstracted from the output of the Network Operations Control Center (NOCC) Pseudo Residual Program. The process used in computing the noise is a "running" standard deviation about a least squares linear curve fit to the most recent 15 samples. Doppler data sample intervals in effect during the period when noise data were accumulated are listed below:

(1) 1 second

(2) 2 seconds

(3) 10 seconds

(4) 60 seconds

Normalization of the noise data to account for different sample intervals is described in detail in Refs. 2 and 3.

III. Evaluation of the Coefficient of the Outer Coronal Density Term

The term in the "ISEDC" doppler noise model (Ref. 1) that describes the noise, hence density, in the outer corona is:

$$A_0 \left[\frac{\beta}{(\sin \alpha)^{1.30}} \right] F(\alpha, \beta)$$

Residuals (in "dB") for the data base are formed between observed and predicted (ISEDC) noise as follows:

$$\Delta(\text{"dB"}) = 10 \log_{10} \left\{ \frac{\text{observed noise}}{\text{ISEDC noise}} \right\}$$

These residuals are then used to produce a standard deviation for the data base of:

$$\sigma = \left\{ \frac{1}{N} \sum_{i=1}^{N} \Delta_i^2 \right\}^{1/2}$$

Computer runs were initiated to obtain the condition:

$$\frac{\partial \sigma}{\partial A_0} = 0$$

This process yielded a value for A_0 of:

$$A_0 = 1.182 \times 10^{-3}$$

and a standard deviation for the data set of

$$\sigma = 1.617 \text{ dB}$$

Figures 1, 2, and 3 present the Viking noise data and the ISEDC model versus DOY or SEP for $A_0 = 1.182 \times 10^{-3}$. Figure 4 is a scatter diagram of observed noise and the ISEDC model for (the same) A_0.

IV. Evaluation of the Coefficient of the Inner Coronal Density Term

The term in the ISEDC model that describes the noise and density in the inner corona is:

$$A_1 \left[\frac{1}{(\sin \alpha)^5} \right]$$

The region of influence of this term is:

$$\text{impact parameter} < 4 \text{ solar radii}$$

All "pass-average" doppler noise values from Helios 1, Helios 2, and Viking which were obtained at impact parameters smaller than 4 solar radii (20 values in all) were compiled in a special data set, and computer runs were performed to obtain the condition:

$$\frac{\partial \sigma}{\partial A_1} = 0$$

This process yielded a value for A_1 of:

$$A_1 = 4.75 \times 10^{-10}$$

and a standard deviation for the data set of

$$\sigma = 1.037 \text{ dB}$$

Figure 5 is a plot of σ versus A_1 while Fig. 6 displays the fit of the observed data to the ISEDC model for $A_1 = 4.75 \times 10^{-10}$.

V. Calibration of the Mean 1976 Equatorial Corona

The functional form of the original ISED model was obtained by integrating the following electron density function:

$$N_e(r) = \frac{A}{r^6} + \frac{B}{r^{2.3}}$$

with

r = heliocentric distance

along the signal path. It is now desired to obtain electron density in the form:

$$N_e(r) = \left\{ \frac{A}{r^6} + \frac{B}{r^{2.30}} \right\} \text{ electrons/cm}^3$$

with

r = heliocentric distance, in solar radii

From Refs. 2 and 6 it is seen that (with r_0 = solar radius, meters):

$$A = \frac{r_e^5}{r_0^6} \left[\frac{8}{3\pi}\right] \left[A_1 \text{ Hz}\right] \left[\frac{7 \times 10^3 \text{m}}{\text{Hz}}\right]$$

$$\times \left[\frac{1.31 \times 10^{17} \text{ electrons/m}^2}{\text{m}}\right]$$

$$= \frac{(214)^5}{(6.95 \times 10^8)} \left[\frac{8}{3\pi}\right] [4.75 \times 10^{-10}]$$

$$\times [7 \times 10^3] [1.31 \times 10^{17}]$$

$$= 2.39 \times 10^{14} \text{ electrons/m}^3$$

$$= 2.39 \times 10^8 \text{ electrons/cm}^3$$

and

$$B = \frac{r_e^{1.3}}{r_0^{2.3}} \left[A_0 \text{ Hz}\right] \left[\frac{7 \times 10^3 \text{ m}}{\text{Hz}}\right]$$

$$\times \left[\frac{1.31 \times 10^{17} \text{ electrons/m}^2}{\text{m}}\right]$$

$$= \frac{(214)^{1.3}}{(6.95 \times 10^8)} [1.182 \times 10^{-3}]$$

$$\times [7 \times 10^3] [1.31 \times 10^{17}]$$

$$= 1.67 \times 10^{12} \text{ electrons/m}^3$$

$$= 1.67 \times 10^6 \text{ electrons/cm}^3$$

so that the 1976 mean equatorial model becomes:

$$N_e(r) = \frac{2.39 \times 10^8}{r^6} + \frac{1.67 \times 10^6}{r^{2.30}}$$

with

N_e = electrons/cm^3

r = heliocentric distance, solar radii

The model yields at 2 solar radii:

$$N_e(2) = 4.1 \times 10^6 \text{ electrons/cm}^3$$

and at 1 AU:

$$N_e(214) = 7.3 \text{ electrons/cm}^3$$

The repeatability of coronal solutions derived from doppler noise is demonstrated via results obtained earlier with Pioneer and Helios data. In Ref. 4, 443 "pass-average" doppler noise values from the 1976 solar conjunctions of Pioneer 10, Pioneer 11, Helios 1, and Helios 2 were combined into a single data set. For the extended corona solution, a signal path integration of $r^{-2.3}$ was assumed, and, as in this article, computer runs were effected to obtain the condition:

$$\frac{\partial \sigma}{\partial A_0} = 0$$

This process yielded (p. 122 of Ref. 4):

$$A_0 = 0.1121 \times 10^{-2}$$

which corresponds to a solution for the extended corona of:

$$N_e = \frac{1.58 \times 10^6}{r^{2.3}} \text{ electrons/cm}^3$$

This solution yields a value for N_e at 1 AU of:

$$N_e(214) = 6.9 \text{ electrons/cm}^3$$

The difference in the coefficient of the $r^{-2.3}$ term (B) between the Viking solution and the Helios/Pioneer solution is thus seen to be 5%.

Table 1 compares this model to various other determinations made in the last decade or so. The critical parameter utilized in this article (7000 meters/Hz, from Ref. 2) was only approximately determined, and a more careful comparison of Viking differenced S-X range to Viking doppler noise could be expected to change the scaling of the density model by up to 10%. The ratio of the coefficients A and B would not change, however, and thus this parameter is included in Table 1 for comparison.

VI. Correlation of Viking Doppler Noise With Heliographic Latitude

In Ref. 5, Pioneer doppler noise obtained for impact parameters at very high heliographic latitudes (up to 80 degrees) was used to indicate a functional dependency of noise and hence density upon heliographic latitude of:

$$F(\phi_s) \sim 10^{-0.9(|\phi_s|/90)}$$

with

ϕ_s = heliographic latitude, degrees

The Viking impact parameter was only at a significant heliographic latitude shortly before and after solar conjunction, and even so, the highest (impact parameter) heliographic latitudes for which pass-average doppler noise was obtained were less than 30 degrees (on DOY 228 and 331). A heliographic latitude of 30 degrees produces a reduction of about 50% according to the results of the Pioneer study. This is typical of the magnitude of routine weekly fluctuations in observed doppler noise (due to solar activity), hence, it is difficult to either corroborate or refute the finding of Ref. 5. Figure 7 compares Viking noise residuals with and without the heliographic latitude correction from DOY 322 to DOY 340.

Using the functional relationship from Ref. 5, one can construct a nonequatorial model for electron density as (approximately):

$$N_e(r) = \left\{ \frac{2.39 \times 10^8}{r^6} + \frac{1.67 \times 10^6}{r^{2.30}} \right\} \left[10^{-0.9(|\phi_s|/90)} \right]$$

with

N_e = electrons/cm^3

r = heliocentric distance, solar radii

ϕ_s = heliographic latitude, degrees

VII. Correlation of Viking Doppler Noise With Earth Observed Solar Activity

By way of brief review, Ref. 6 assumed that doppler noise could be correlated with Earth-observed sunspot activity (R_Z) by rotating $R_Z \pm 6\text{-}3/4$ days (subtract for signal paths east of the Sun and add for signal paths west of the Sun) so as to put the "observed" region on the solar limb and propagating

towards the signal closest approach point. Then a finite propagation time was considered:

$$t_\tau \text{ (days)} = A_2 \sin \alpha$$

$$\cong A_2 \alpha$$

A_2 was varied to minimize the noise residuals, resulting in:

$$A_2 = 12 \text{ days/rad}$$

which was subsequently seen to be an "averaged" velocity of propagation of:

$$V \sim 120 \text{ km/s}$$

Callahan (Ref. 17), in a similar fashion rotated R_Z ±7 days, but did not allow for a finite propagation time. He found "moderate" correlation between spectral amplitudes and R_Z for 6 days (east of the Sun) and 10 days (west of the Sun), both results being entirely consistent with the assumption of a finite propagation time. A possibly better assumption in any future attempts of this type would be:

$$t_\tau \approx \int_0^a \frac{dr}{V_W(r)}$$

where:

a = closest approach distance

$V_W(r)$ = solar wind speed

Figure 8 presents Viking doppler noise residuals versus XR_Z (Ref. 6), which is the smoothed, phased Sunspot Index. Some regions such as that from DOY 270 to 315, appear to show some correlation. On the other hand, the region surrounding DOY 264 evidences a very strong negative correlation.

VIII. Conclusions

The authors believe that this article demonstrates the feasibility of using S-band doppler rms phase fluctuations from any (or all) spacecraft in solar conjunction phases to (more or less) continuously calibrate electron density in the solar corona. In addition, doppler rms phase fluctuations would appear to be a very useful tool in probing the time scale of electron density fluctuations (Ref. 2) and correlating electron density and density fluctuations with Earth-observed solar activity.

References

1. Berman, A. L., Wackley, J. A., Rockwell, S. T., and Kwan, M., "Viking Doppler Noise used to Determine the Radial Dependence of Electron Density in the Extended Corona," in *The Deep Space Network Progress Report 42-38,* Jet Propulsion Laboratory, Pasadena, California, April 15, 1977 (published in this volume).

2. Berman, A. L., "Proportionality Between Doppler Noise and Integrated Signal Path Electron Density Validated by Differenced S-X Range," in *The Deep Space Network Progress Report 42-38* (this volume), Jet Propulsion Laboratory, Pasadena, California, April 15, 1977 (published in this volume).

3. Berman, A. L., "A Comprehensive Two-Way Doppler Noise Model for Near-Real-Time Validation of Doppler Data," in *The Deep Space Network Progress Report 42-37,* Jet Propulsion Laboratory, Pasadena, California, February 15, 1977.

4. Berman, A. L., Wackley, J. A., and Rockwell, S. T., "The 1976 Helios and Pioneer Solar Conjunctions – Continuing Corroboration of the Link Between Doppler Noise and Integrated Signal Path Electron Density," in *The Deep Space Network Progress Report 42-36,* Jet Propulsion Laboratory, Pasadena, California, 15 December 1976.

5. Berman, A. L., Wackley, J. A., Rockwell, S. T., and Yee, J. G., "The Pioneer 11 1976 Solar Conjunction: A Unique Opportunity to Explore the Heliographic Latitudinal Variations of the Solar Corona," in *The Deep Space Network Progress Report 42-35,* Jet Propulsion Laboratory, Pasadena, California, 15 October 1976.

6. Berman, A. L., and Wackley, J. A., "Doppler Noise Considered as a Function of the Signal Path Integration of Electron Density," in *The Deep Space Network Progress Report 42-33,* Jet Propulsion Laboratory, Pasadena, California, 15 June 1976.

7. Berman, A. L., "Analysis of Solar Effects Upon Observed Doppler Data Noise During the Helios 1 Second Solar Conjunction," in *The Deep Space Network Progress Report 42-32,* Jet Propulsion Laboratory, Pasadena, California, 15 April 1976.

8. Berman, A. L., and Rockwell, S. T., "Correlation of Doppler Noise During Solar Conjunctions with Fluctuations in Solar Activity," in *The Deep Space Network Progress Report 42-30,* Jet Propulsion Laboratory, Pasadena, California 15 December 1975.

9. Berman, A. L., and Rockwell, S. T., "Analysis and Prediction of Doppler Noise During Solar Conjunctions," in *The Deep Space Network Progress Report 42-30,* Jet Propulsion Laboratory, Pasadena, California, 15 December 1975.

10. Weisberg, J. M., Rankin, J. M., Payne, R. R., and Counselman III, C. C., "Further Changes in the Distribution of Density and Radio Scattering in the Solar Corona," *The Astrophysical Journal,* 209, October 1, 1976.

11. Anderson, J. D., et al., "Experimental Test of General Relativity Using Time Delay Data from Mariner 6 and Mariner 7," *The Astrophysical Journal,* August 15, 1975.

12. Muhleman, D. O., Anderson, J. D., Esposito, P. B., and Martin, W. L., "Radio Propagation Measurements of the Solar Corona and Gravitational Field; Applications to Mariner 6 and 7," in *Proceedings of the Conference on Experimental Tests of Gravitational Theories,* California Institute of Technology, Pasadena, California, November, 1970.

13. Dutcher, G. L., *A Communication Channel Model of the Solar Corona and the Interplanetary Medium,* CSRT-69-1, Center for Space Research, Massachusetts Institute of Technology, 1969.

14. Saito, Kuniji, "A Non-Spherical Axisymmetric Model of The Solar K Corona of The Minimum Type," *Annals of The Tokyo Astronomical Observatory,* University of Tokyo, Second Series, Volume XII, Number 2, Mitaka, Tokyo, 1970.

15. Newkirk, G., "Structure of The Solar Corona," in The *Ann. Rev. Astron. Astrophys.*, 1967.

16. Stelzreid, C. T., "A Faraday Rotation Measurement of a 13 CM Signal in the Solar Corona," Technical Report 32-1401, Jet Propulsion Laboratory, Pasadena, California, July 15, 1970.

17. Callahan, P. S., "Observations of The Solar Wind Turbulence Near The Sun," Doctoral Thesis, 1975, California Institute of Technology, Pasadena, California.

Table 1. Coronal model comparisons

Source	Ref.	$A \times 10^{-8}$	$B \times 10^{-6}$	A/B	ξ	$N_e \times 10^{-6}$ at $2r_0$	N_e at 1 AU	Solar Cycle
Berman & Wackley[a]		2.39	1.67	143	0.30	4.1	7.3	Min
Berman & Wackley[b]			1.58		0.3		6.9	Min
Weisberg, et al.	10		1.60		0.3		7.0	Min
Weisberg, et al.	10		0.94		0.1		12.1	Min
Anderson, et al.	11	0.69	0.54	127	0.05	1.2	9.0	
Muhleman, et al.	12	1.92	1.41	136	0.41	3.3	3.4	Max
Muhleman, et al.	12	1.30	1.15	113	0.3	2.3	5.0	
Muhleman, et al.	12	0.80	0.51	156	0.3	1.4	2.2	Max
Dutcher	13						6	
Saito	14	1.58	2.51	63	0.5	2.9	3.8	
Blackwell, et al.	11	2.62	2.07	126	0.33	4.5	7.7	Max
Blackwell, et al.	11	1.01	2.01	50	0.33	2.0	7.5	Min
Blackwell & Petford	11	1.18	1.46	81	0.3	2.1	6.4	Min
Newkirk	15					5.6	5.0	Max
Newkirk	15					2.8	2.5	Min
Allen – Baumbach	16	1.55	1.00	155	0.0	2.7	21.8	

[a]Viking data.

[b]Pioneer and Helios data.

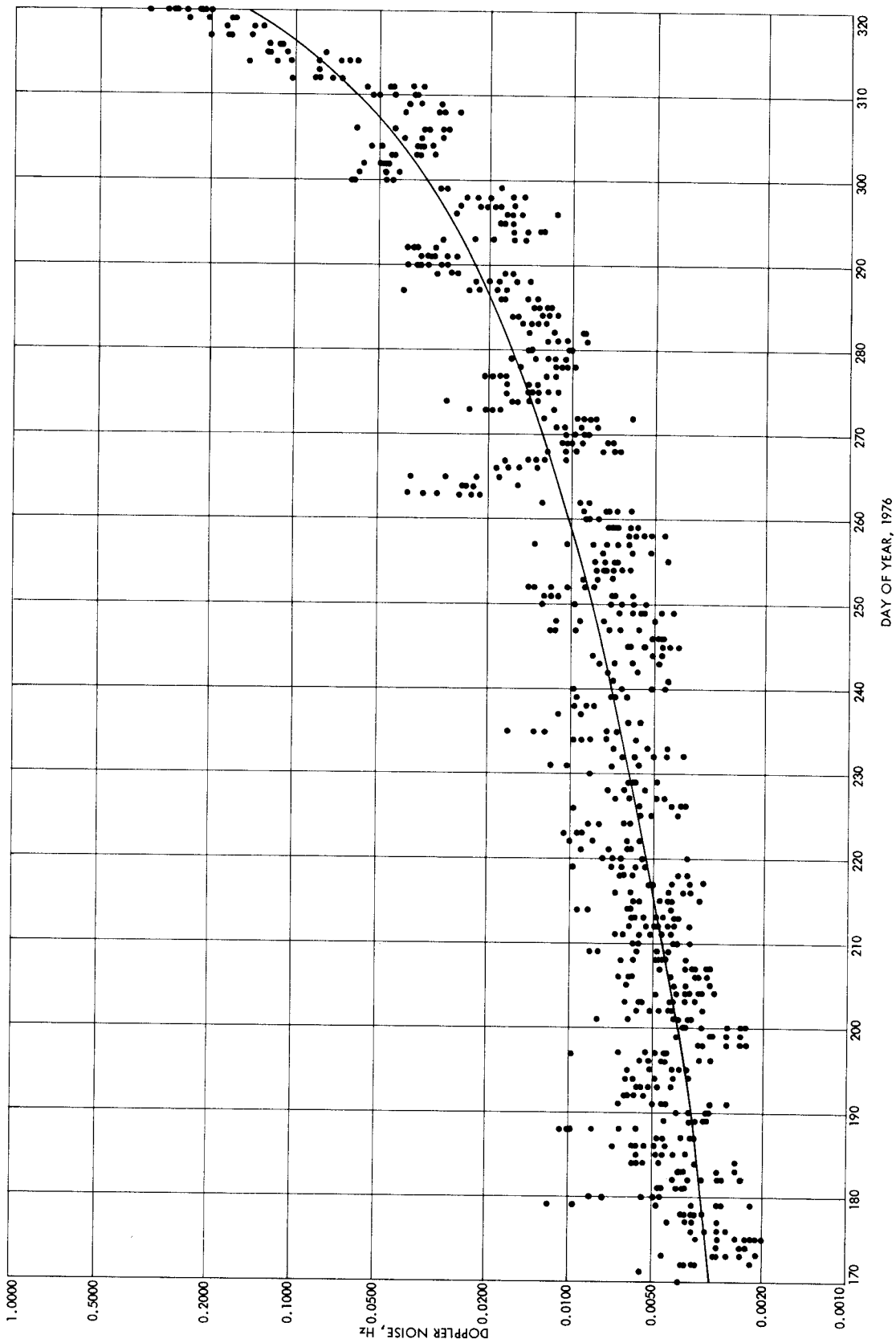

Fig. 1. Viking doppler noise and the ISEDC model vs day of year (170 to 320)

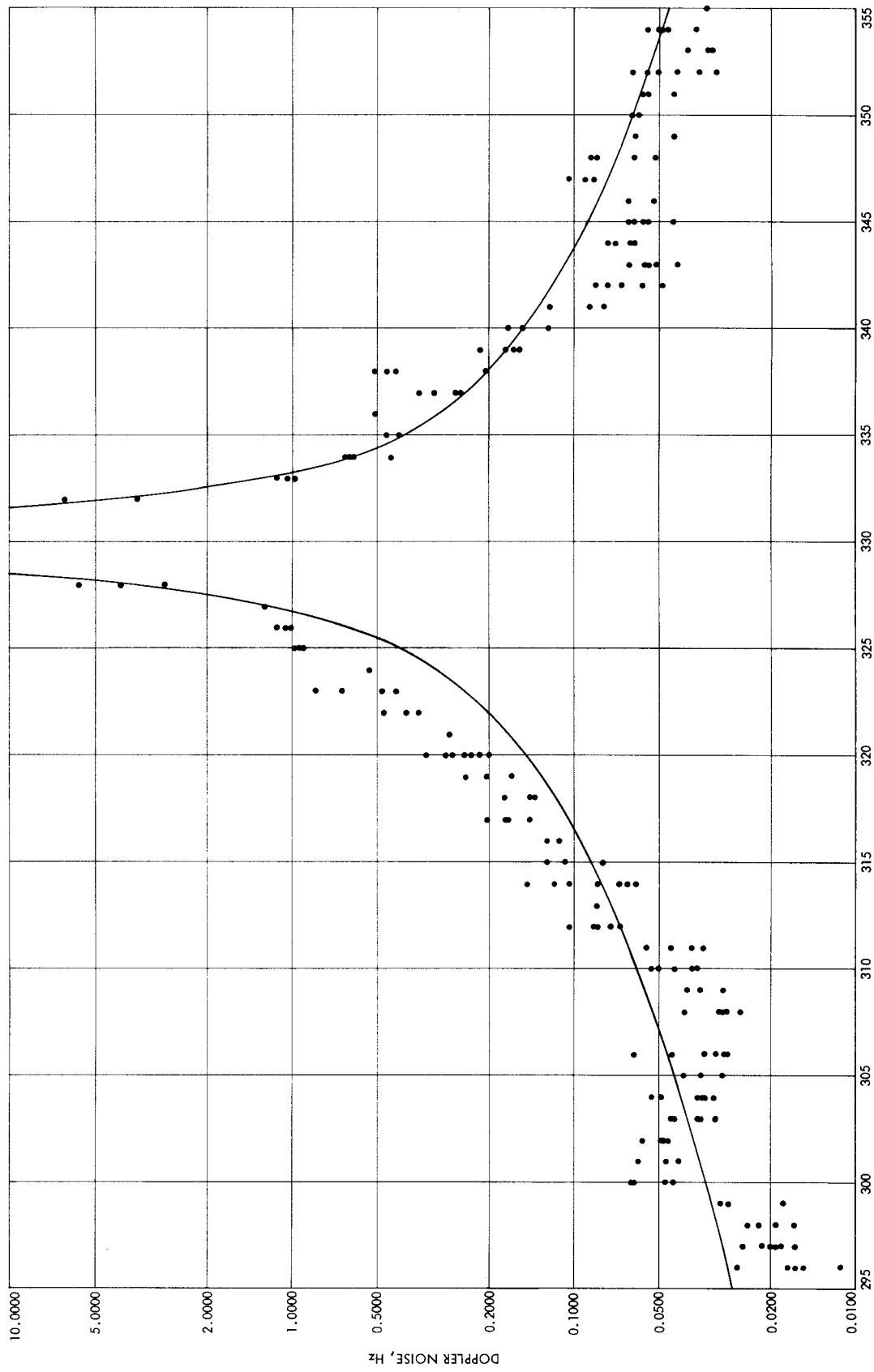

Fig. 2. Viking doppler noise and the ISEDC model vs day of year (295 to 355)

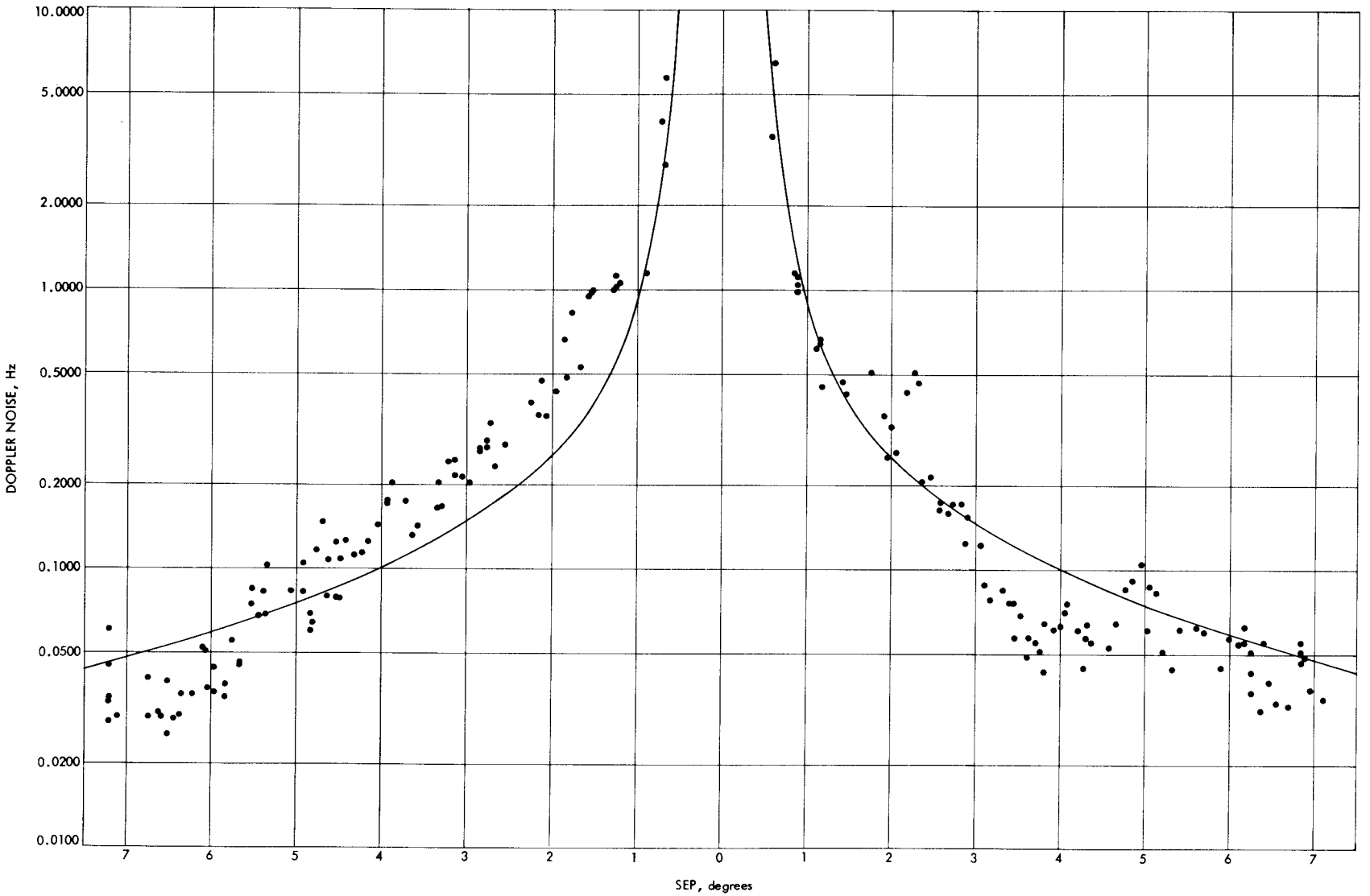

Fig. 3. Viking doppler noise and the ISEDC model vs SEP angle

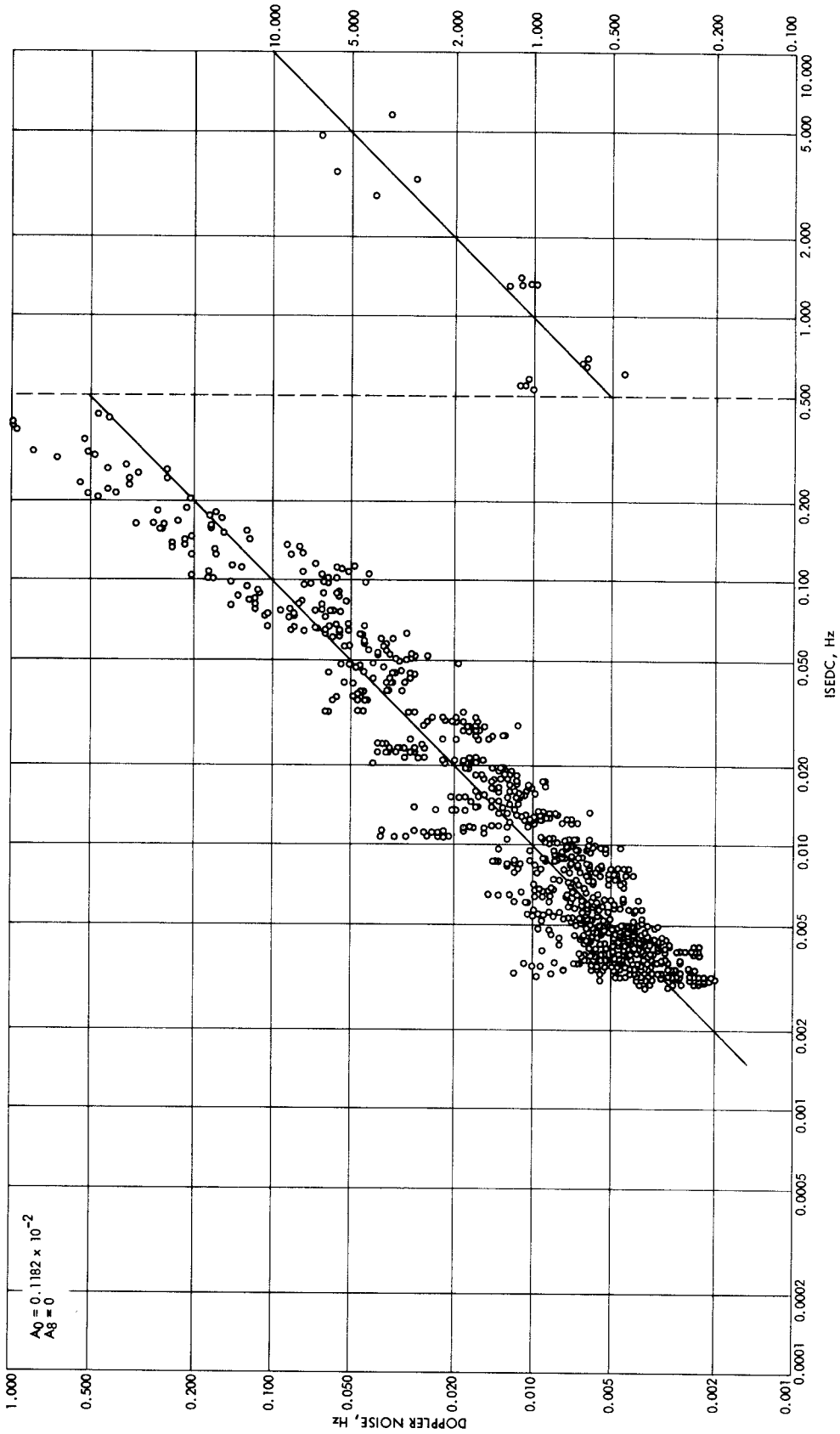

Fig. 4. Viking doppler noise vs the ISEDC model

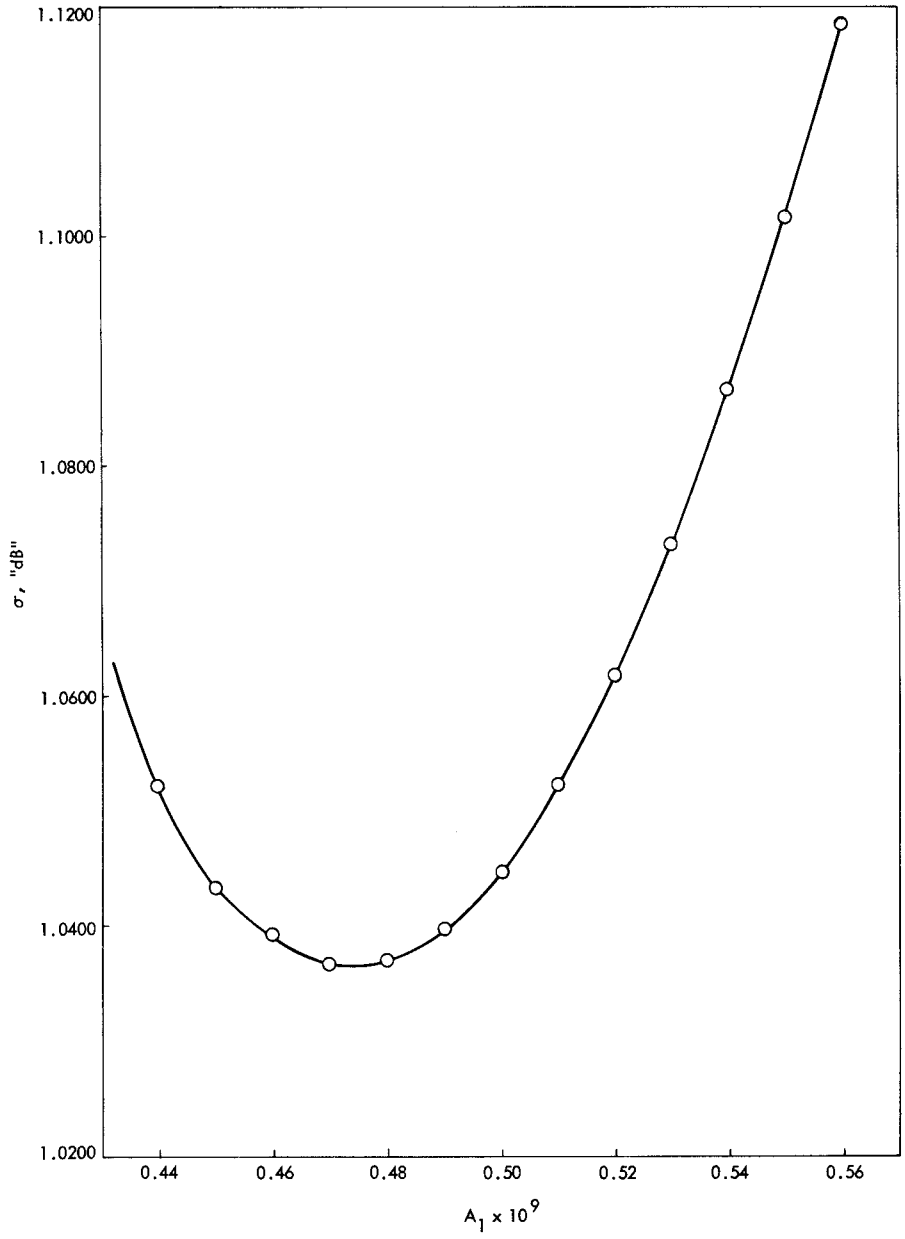

Fig. 5. Low SEP Viking and Helios doppler noise fit vs A_1

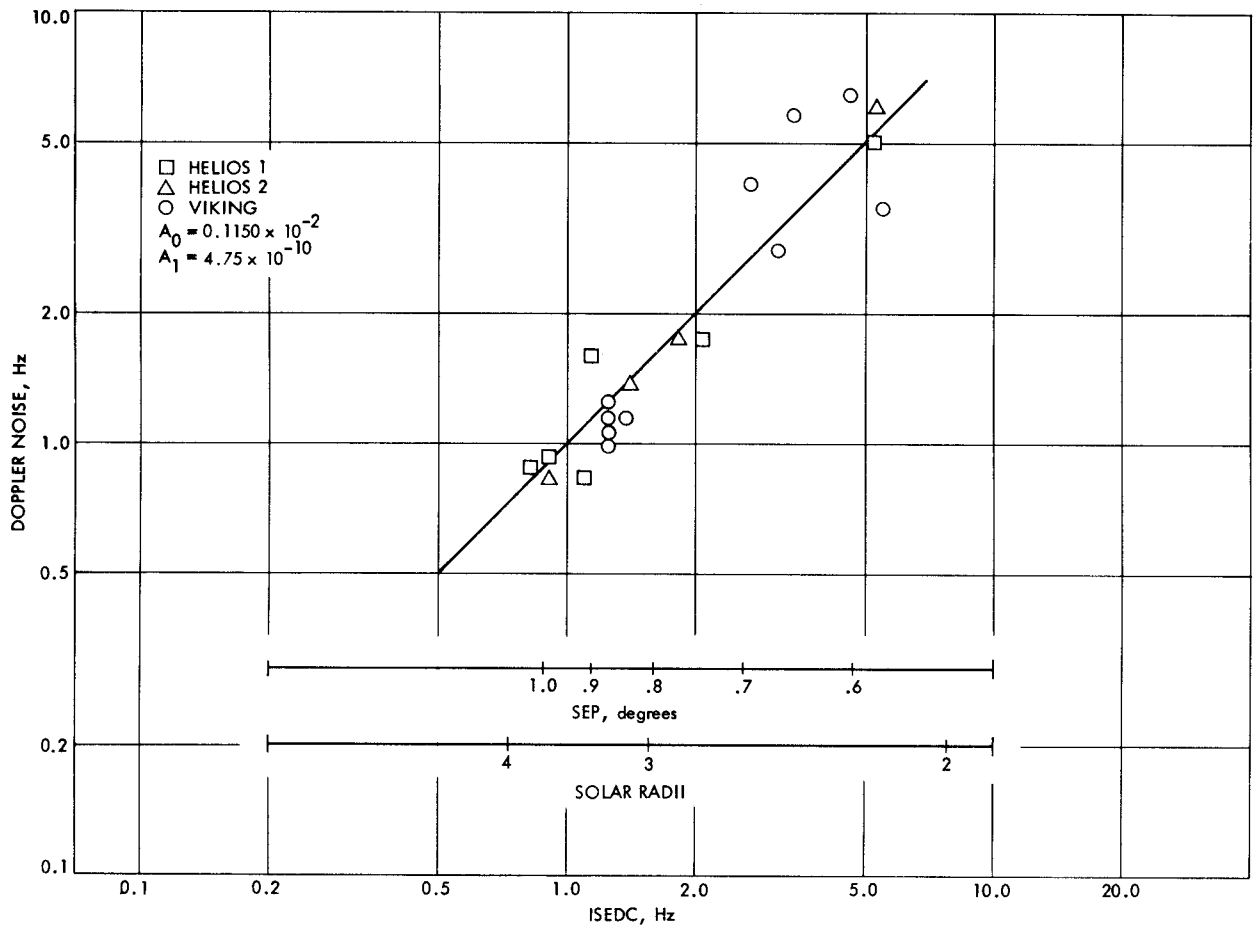

Fig. 6. Viking and Helios doppler noise fit to ISEDC between 2 to 4 solar radii

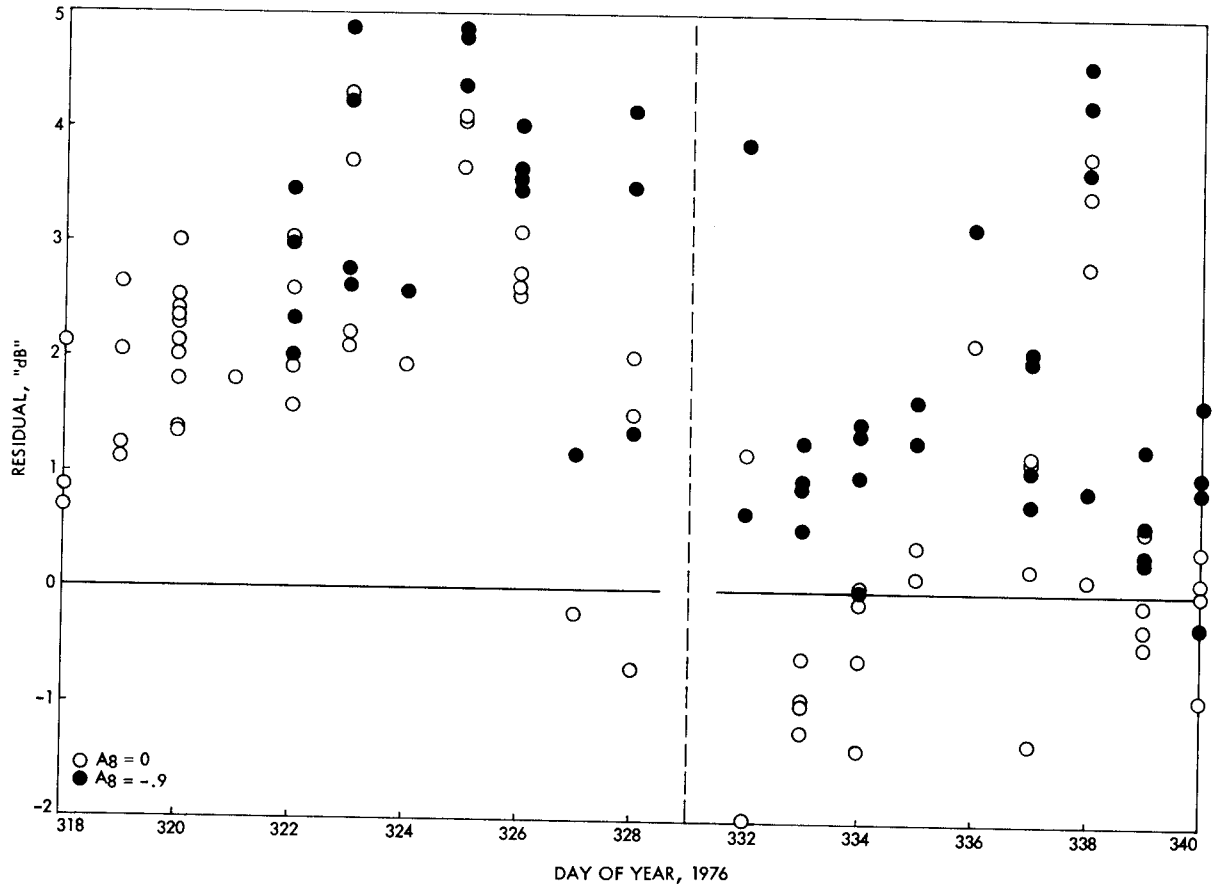

Fig. 7. ISEDC residuals with and without heliographic latitude correction

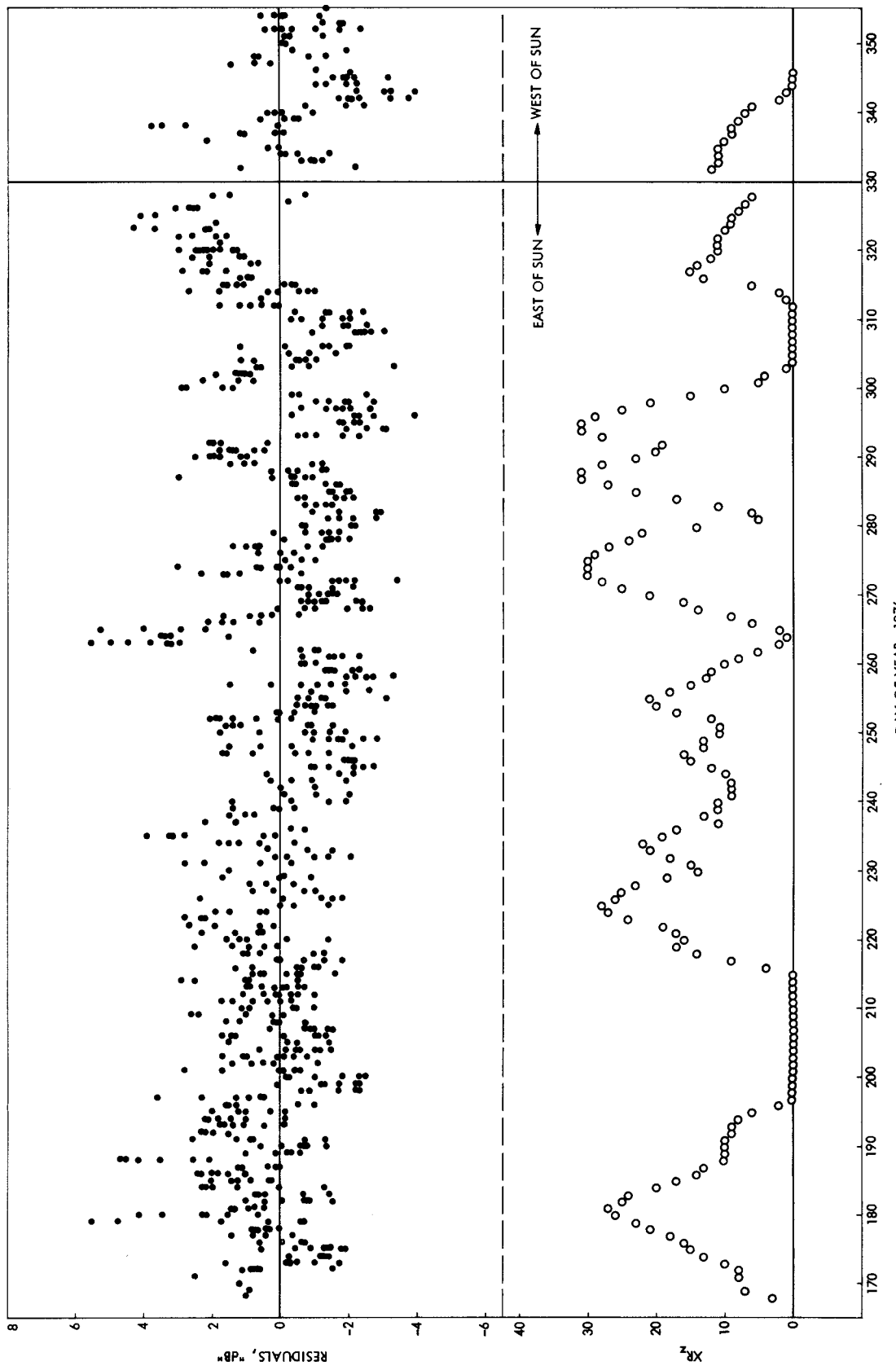

Fig. 8. Viking doppler noise residuals and phased/smoothed sunspots vs day of year